Lava field evolution and emplacement dynamics of the 2014–2015 basaltic fissure eruption at Holuhraun, Iceland

G.B.M. Pedersen [a,*], A. Höskuldsson [a], T. Dürig [a], T. Thordarson [b], I. Jónsdóttir [a], M.S. Riishuus [a], B.V. Óskarsson [a], S. Dumont [a,c], E. Magnusson [a], M.T. Gudmundsson [a], F. Sigmundsson [a], V.J.P.B. Drouin [a], C. Gallagher [a,d], R. Askew [a], J. Gudnason [a], W.M. Moreland [a], P. Nikkola [a], H.I. Reynolds [a], J. Schmith [a,e], the IES eruption team

[a] Nordic Volcanological Center, Institute of Earth Sciences, University of Iceland, Sturlugata 7, 101 Reykjavík, Iceland
[b] Faculty of Earth Sciences, University of Iceland, Sturlugata 7, 101 Reykjavík, Iceland
[c] Instituto Dom Luiz, University of Beira Interior, Rua Marques d'Avila e Boloma, 6201-001 Covilhã, Portugal
[d] Department of Earth Sciences, Science Labs, Durham University, Elvet Hill, Durham DH1 3LE, United Kingdom
[e] Department of Geosciences and Natural Resource Management, University of Copenhagen, Rolighedsvej 23, 1958 Frederiksberg C, Denmark

A B S T R A C T

The 6-month long eruption at Holuhraun (August 2014–February 2015) in the Bárðarbunga-Veiðivötn volcanic system was the largest effusive eruption in Iceland since the 1783–1784 CE Laki eruption. The lava flow field covered ~84 km^2 and has an estimated bulk (i.e., including vesicles) volume of ~1.44 km^3. The eruption had an average discharge rate of ~90 m^3/s making it the longest effusive eruption in modern times to sustain such high average flux. The first phase of the eruption (August 31, 2014 to mid-October 2014) had a discharge rate of ~350 to 100 m^3/s and was typified by lava transport via open channels and the formation of four lava flows, no. 1–4, which were emplaced side by side. The eruption began on a 1.8 km long fissure, feeding partly incandescent sheets of slabby pāhoehoe up to 500 m wide. By the following day the lava transport got confined to open channels and the dominant lava morphology changed to rubbly pāhoehoe and 'a'ā. The latter became the dominating morphology of lava flows no. 1–8. The second phase of the eruption (Mid-October to end November) had a discharge of ~100–50 m^3/s. During this time the lava transport system changed, via the formation of a <1 km^2 lava pond ~1 km east of the vent. The pond most likely formed in a topographical low created by a the pre-existing Holuhraun and the new Holuhraun lava flow fields. This pond became the main point of lava distribution, controlling the emplacement of subsequent flows (i.e. no. 5–8). Towards the end of this phase inflation plateaus developed in lava flow no. 1. These inflation plateaus were the surface manifestation of a growing lava tube system, which formed as lava ponded in the open lava channels creating sufficient lavastatic pressure in the fluid lava to lift the roof of the lava channels. This allowed new lava into the previously active lava channel lifting the channel roof via inflation. The final (third) phase, lasting from December to end-February 2015 had a mean discharge rate of ~50 m^3/s. In this phase the lava transport was mainly confined to lava tubes within lava flows no. 1–2, which fed breakouts that resurfaced >19 km^2 of the flow field. The primary lava morphology from this phase was spiny pāhoehoe, which superimposed on the 'a'ā lava flows no. 1–3 and extended the entire length of the flow field (i.e. 17 km). This made the 2014–2015 Holuhraun a paired flow field, where both lava morphologies had similar length. We suggest that the similar length is a consequence of the pāhoehoe is fed from the tube system utilizing the existing 'a'ā lava channels, and thereby are controlled by the initial length of the 'a'ā flows.

1. Introduction

Basaltic magmatism is the principal component of the volcanism in Iceland. The volume of Holocene mafic lava has been estimated to be ~370 km^3, thus, giving an average lava production rate of ~3.5 km^3 per century (Thordarson and Höskuldsson, 2008; Thordarson and Larsen, 2007). These effusive eruption episodes represent a wide spectrum of eruption style and magnitude, of which small to medium-sized (<1 km^3) eruptions recur with decadal frequency, whereas large volume (≥1 km^3) effusive events have a repose periods of a few hundred years (Thordarson and Höskuldsson, 2008). In the last 50 years only small volume effusive eruptions have been witnessed in Iceland, e.g. the Hekla eruptions from 1970, 1980–1981, 1991 and 2000 (≤0.2 km^3) and the 9 Krafla eruptions in 1975–1984 (~0.25 km^3, Rossi, 1997; Höskuldsson et al., 2007).

* Corresponding author at: Nordic Volcanological Center, Institute of Earth Sciences, University of Iceland, Sturlugata 7, 101 Reykjavík, Iceland.
E-mail address: gro@hi.is (G.B.M. Pedersen).

From August 31, 2014 to February 27, 2015 the eruption at Holuhraun formed a lava flow field covering 84 km^2, with a bulk volume of 1.44 km^3 as calculated from the difference of pre- and post-eruption digital elevation models (Höskuldsson et al., 2016). This makes the 2014–2015 eruption 5–10 times larger than the previous effusive eruptions observed in recent decades in Iceland. The 2014–2015 Holuhraun eruption therefore provides an opportunity to improve our understanding of large effusive eruptions. Near continuous on-site monitoring of this six-month long event has enabled detailed documentation of the modes of lava transport and emplacement, along with mapping of the flow field growth and evolution. In addition, it provided the opportunity to effectively link lava emplacement mechanisms to flow morphology. Here we present a compilation of the results from these observations.

1.1. Volcanic architecture of mafic lava flow fields

Flow fields formed in effusive basaltic eruptions develop lava channels and lava tubes that transport the lava from the vent to the active flow front where lava dispersion and active growth of the lava flow field takes place (e.g. Self et al., 1998; Harris and Rowland, 2015). The architecture of lava flow fields is variable and can encompass one or a collection of several lava flows produced during the eruption. One lava flow is a regional subunit and is defined as one outpouring of lava originating from a specific part of the vents or formed during an eruptive phase (Thordarson and Self, 1998). Lava flows consists of flow lobes (sometimes referred to as "flow units"), which are the smallest identifiable parcels of lava (Self et al., 1998; Thordarson and Self, 1998; Harris and Rowland, 2015). A breakout is a lobe originating from the molten interior of an active lava lobe. It may occur through a crack at the front or the side of the lobe (Thordarson and Self, 1998). In this article we also use the term distributary center for central locations, where the pathways bifurcate and thereby distribute lava in different directions over a period of time.

Since late 19th century, it has been common practice, to categorize mafic lava flows into two morphological end-member types; namely 'a'ā and pāhoehoe, due to their distinct surface flow structures (e.g. Macdonald, 1953; Swanson, 1973; Kilburn, 1981; Lipman and Banks, 1987; Rowland and Walker, 1990; Harris et al., 2017).

Pāhoehoe flows have coherent, smooth, billowy or ropy surfaces and are normally comprised of multiple flow lobes (e.g. Macdonald, 1953; Self et al., 1998; Harris et al., 2017). Depending on the type of pāhoehoe morphology, the lobe size can vary from tens of centimeters to hundreds of meters in length and width (see Suppl. Table 1, Thordarson and Self, 1998). Their thicknesses vary from centimeters to tens of meters in thickness (e.g. Thordarson and Self, 1998). In small Hawaiian eruptions the breakouts are relatively thin (cm to dm thick) but commonly increase their thickness 5- to 10-fold via inflation (Hon et al., 1994). Pāhoehoe flows grow via sequential lobe breakouts and inflation at active flow fronts and thereby create morphologies such as lava tubes, tumuli, lava rises, lava-rise pits and inflation clefts (Walker, 1991; Hon et al., 1994; Self et al., 1998; Thordarson and Self, 1998).

An 'a'ā lava is enveloped by rubble composed of jagged, spinous clasts of clinker formed by viscous tearing that typically are centimeters to decimeters across. The clinker is rafted towards the flow front where it is dislodged in a conveyor-belt motion. Typical 'a'ā flow thicknesses vary from 0.5–20 m (Macdonald, 1953; Harris and Rowland, 2015). Inflation and lava tube formation have also been recorded in 'a'ā flows (e.g. Calvari and Pinkerton, 1998) though open channel systems are more common. The term lava rise was defined as a horizontal uplift of surface crust in pāhoehoe flows (Walker, 1991), and in order to avoid confusion, we use the term inflation plateau to describe horizontal uplift of surface crust within an 'a'ā flow. The inflation plateau is a type of lava tube, which typically is confined by the channel of the 'a'ā flow and the inflation is thereby delimited by the shear zone and is thereby detached from the levees of the 'a'ā flow.

Basaltic lava flows may change morphology as they flow away from the vent, commonly changing from pāhoehoe to 'a'ā downstream. This change in morphology within a flow has been defined as lava transition, e.g. a pāhoehoe-'a'ā transition (Macdonald, 1953). Here we adopt Macdonald (1953) definition for lava transition, meaning that the morphology of the flow change along a single flow, generally occurring at the front of advancing lobes, where most crust is being formed (Hon et al., 2003). The morphologies are not systematically related to geochemical differences, but rather to variations in the lava rheology, shear strain and flow dynamics (e.g. Macdonald, 1953; Peterson and Tilling, 1980; Rowland and Walker, 1990; Cashman et al., 1999; Hon et al., 2003). Hence, molten lava which reach the critical relation between viscosity and shear strain will produce 'a'ā crust, while it with lower viscosity or shear strain will produce pāhoehoe (Peterson and Tilling, 1980; Hon et al., 2003). When crust has formed, its morphology will not change. Thus, a piece of 'a'ā crust cannot change into a pāhoehoe crust or vice versa. A lava flow has a considerable range in viscosity values and rates of shear strain, and hence the morphology is recording the conditions of the lava, when the surface crust was forming at a particular location, while the interior of the flow may record later emplacement conditions (Jurado-Chichay and Rowland, 1995).

2. Geological setting

The Bárðarbunga-Veiðivötn volcanic system is one of Iceland's largest volcanic systems. It consists of a glacier-covered central volcano and a 190-km-long, mostly subaerial, fissure swarm (Fig. 1, Einarsson and Sæmundsson, 1987; Johannesson and Sæmundsson, 1998; Thordarson and Larsen, 2007, Hjartardóttir et al., 2015; Sigmarsson and Halldórsson, 2015). The central volcano is located within the northwestern part of the Vatnajökull ice cap and features a 8 km by 13 km wide and 500–700 m-deep caldera (Gudmundsson et al., 2016).

The eruption history of the Bárðarbunga-Veiðivötn volcanic system in the Holocene is not fully known, however the eruption frequency is suggested to be ~5 eruptions per century (Óladóttir et al., 2011). Tephrachronological studies of ice and soil, along with written records from the last 1000 years has verified 22 eruptions on the south western fissure swarm in the last 9000 years, while the fissure swarm to the north is less well-known, but suggest that >10 eruptions have occurred (Óladóttir et al., 2011; Larsen et al., 2015).

The most recent pre-2014 lava flow fields on the north arm of the fissure swarm are the Holuhraun lavas of 1797 CE (Holuhraun I) and 1867 CE (Holuhraun II). These basaltic lavas have chemical signatures that indicate affinity with the Bárðabunga-Veiðivötn volcanic system (Hartley and Thordarson, 2013; Sigmarsson and Halldórsson, 2015). Holuhraun I erupted from a 1.5 km long fissure 5–6 km north of Dyngjujökull, whereas Holuhraun II erupted just outside the Dyngjujökull glacier.

The 2014–2015 Holuhraun lavas were, like the Holuhraun I flows, emplaced on the central part of the floodplain, 6 km north of the Dyngjujökull glacier. This floodplain is largely covered by glacial and fluvial deposits from Jökulsá á Fjöllum river, and has a regional dip of ~1° to the northeast. It features decimeter to meter scale banks, bars and river terraces, which close to the central parts of the river channel may have relief up to 7 m.

2.1. Overview of 2014–2015 Holuhraun eruption

On August 16, 2014 an intense seismic swarm began beneath the ice-covered Bárðarbunga volcano. The initial seismic activity occurred in several clusters, but over the following 11 days it concentrated along a lineament and propagated 48 km to the northeast, terminating on the floodplain, 8 km north of the outlet glacier Dyngjujökull (e.g. Sigmundsson et al., 2014; Hjartardóttir et al., 2016; Ágústdóttir et al., 2016). Concurrent subglacial eruptions are inferred to have taken place along this lineament because ice cauldrons were identified

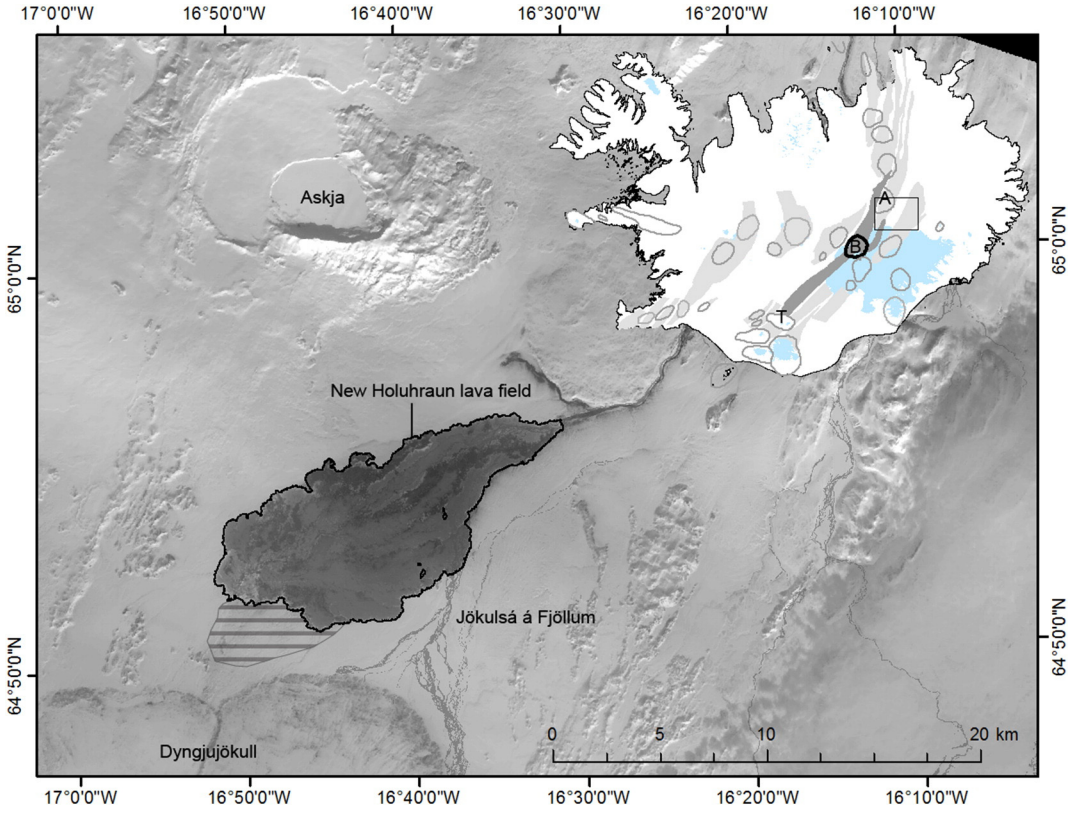

Fig. 1. The new Holuhraun lava field imaged by a LANDSAT on April 2, 2015, 33 days after the eruption stopped. The Holuhraun lava field is located on a flood plain. It is situated south of Askja volcano and north of Dyngjujökull, which is an outlet glacier from the Vatnajökull ice cap. The hatched area marks the region, where the old Holuhraun lava field hindered tracking of the new Holuhraun lava field. The glacial river Jökulsá á Fjöllum is located south and east of the new Holuhraun lava field. The location of Holuhraun, within Iceland itself, is marked by the black box on the inset map of Iceland in the upper right corner. The glaciers are shown in blue and the Icelandic volcanic systems are marked in gray (Einarsson and Sæmundsson, 1987; Hjartardóttir et al., 2016). The fissure swarm of the Bárðarbunga-Veiðivötn volcanic system is highlighted in dark gray and its central volcano is marked with a black circle, which is noted with the letter B. The Torfajökull and Askja central volcanoes of are marked with letter T and A, respectively. (For interpretation of the references to color in this figure legend, the reader is referred to the web version of this article.)

at the ice surface in 3 places (Reynolds et al., 2015; Sigmundsson et al., 2014; Eibl et al., 2017).

The first subaerial eruption took place at midnight on August 29, 2014 (Suppl. Table 2). Lava erupted for 4 h from a 600 m-long fissure that opened up at the old cone row from the Holuhraun I event. After a 24 h hiatus, the fissure was re-activated on August 31 (~5:00 GMT), lengthening to 1.8 km in the process. The fissure was continuously active until the February 27, 2015 (Suppl. Table 2). Another subaerial fissure eruption took place 2 km south of the main fissure on September 5 (~07:00 GMT) and lasted until September 6. During the volcanic unrest, a 65 m deep gradual caldera subsidence took place at the Bárðarbunga central volcano (Gudmundsson et al., 2016), which, like the eruption, stopped after 6 months (Suppl. Table 2).

The main eruption was characterized by high average flux of ~90 m^3/s and the maximum discharge rate during the first phase of the eruption is estimated to have been ≥350m^3/s (Höskuldsson et al., 2015; Höskuldsson et al., 2016; Pedersen et al., 2015; Gislason et al., 2015; Thordarson et al., 2015), dropping to ~60–70 m^3/s at the end of December, after four months of continuous eruption. The discharge rate continued to decrease from mid- January until the end (Coppola et al., 2017; Thordarson et al., 2015). In total the bulk volume of erupted lava has been estimated to be 1.44 km^3 based on pre and post-eruption topography derived from stereo-photogrammetry (Höskuldsson et al., 2016).

3. Data acquisition and methods

This study is based on field measurements, airborne data, and satellite observations (Suppl. Table 2). The field monitoring was carried out almost daily during the first three months of the eruption, but was reduced to weekly surveillance during the winter season due to difficult weather conditions and limited daylight. The instruments used for field data acquisition included Global Positioning System (GPS) measurements and images from GoPro cameras installed on 4 × 4 vehicles for accurate positioning of the track and documentation of the flow field margins on the time scales of a day to a few days. The georeferenced video footage from the GoPro cameras allowed manual classification of the lava margin morphology and occurrence of incandescence. We tracked the western, northern and eastern lava margins, but the pre-existing Holuhraun lava field hindered tracking of the southern margin (Fig. 1). On September 7 the lava reached the Jökulsá á Fjöllum river, and hereafter, only the northern and western lava margins were accessible for observations. The lava margin morphology recorded by the GoPro, was analyzed as a function of the distance from the vent and the local flow velocity using the proximity toolbox within the ArcGIS software. The distance from the vent was calculated to each georeferenced GoPRO frame and the flow velocity was obtained by dividing the distance with the time between consecutive GoPro frames. In addition to the tracking with GoPro cameras, time-lapse videos were taken of the advancing flow, recording changes in lava lobe emplacement on the time scales of 1–6 h.

The size of the lava field made remote sensing data extremely important for monitoring the growth of the lava flow field, and aerial and satellite data provided complementary observations throughout the eruption (e.g. Jónsdóttir et al., 2014). Of particular importance for observations on the lava morphology were X-band images from the airborne, non-polarimetric Synthetic Aperture Radar (SAR) onboard the aircraft TF-SIF. The incidence angle of the radar during these

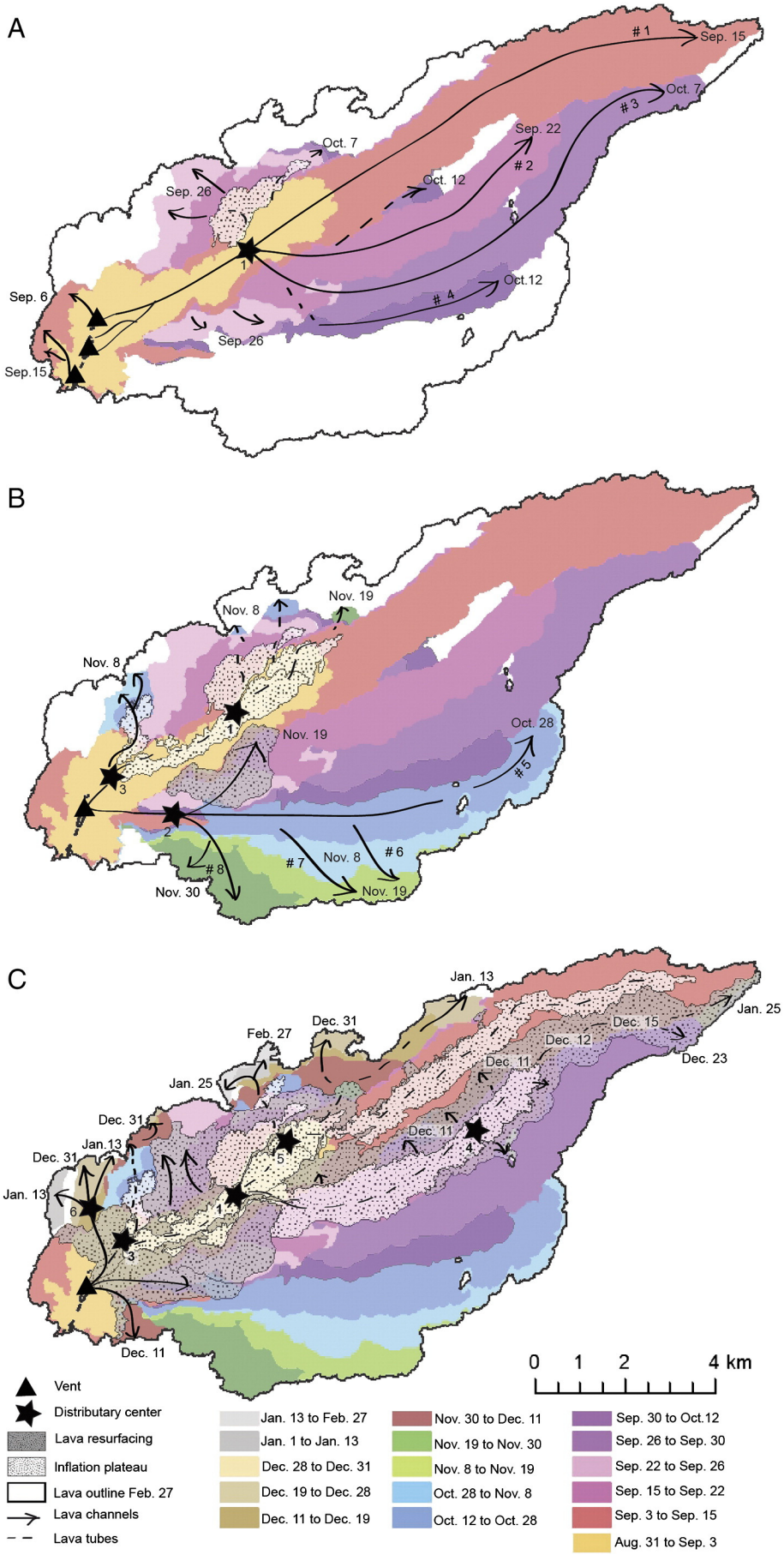
A
1
Sep. 15
Oct. 7
3
Sep. 22
2
Oct. 7
Oct. 12
Sep. 26
1
Oct.12
4
Sep. 6
Sep. 26
Sep.15
B
Nov. 8
Nov. 19
Nov. 8
Nov. 19
Oct. 28
5
1
3
2
8
7
Nov. 8
6
Nov. 30
Nov. 19
C
Jan. 13
Jan. 25
Dec. 31
Feb. 27
Dec. 15
Dec. 12
Dec. 11
Dec. 23
Jan. 25
Dec. 31
Jan.13
Dec. 31
Dec. 11
5
4
Jan. 13
6
1
3
Dec. 11
0 1 2 4 km
Vent
Distributary center
Lava resurfacing
Inflation plateau
Lava outline Feb. 27
Lava channels
Lava tubes
Jan. 13 to Feb. 27
Jan. 1 to Jan. 13
Dec. 28 to Dec. 31
Dec. 19 to Dec. 28
Dec. 11 to Dec. 19
Nov. 30 to Dec. 11
Nov. 19 to Nov. 30
Nov. 8 to Nov. 19
Oct. 28 to Nov. 8
Oct. 12 to Oct. 28
Sep. 30 to Oct.12
Sep. 26 to Sep. 30
Sep. 22 to Sep. 26
Sep. 15 to Sep. 22
Sep. 3 to Sep. 15
Aug. 31 to Sep. 3

Table 1
Topographic and geometric characteristics of lava flows, inflation plateaus and resurfaced areas. Z_min and Z_max is the minimum and maximum elevation measured along the lava flows.

		Start	End	Days	Length [km]	Velocity average [km/day]	Average width [km]	Z_Min [m]	Z_Max [m]	Area [km^2]	**Cumm. lava field [km^2]**	**Cumm. inflation [km^2]**	**Cumm. resurfacing [km^2]**
Phase 1	Lava flow no. 1	Aug. 31	Sep. 15	15	16.95	1.13	1.64	713	811	27.86			
	Lava flow no. 2	Sep. 15	Sep. 22	7	11.76	1.08	1.36	734	811	10.26			
	Overflow	Sep. 22	Sep. 26							4.51			
	Lava flow no. 3	Sep. 26	Oct. 7	15	16.30	0.81	1.03	720	811	12.46			
	Lava flow no. 4	Oct. 7	Oct. 12	5	11.00	1.23	0.52	751	811	3.21			
	Inflation plateau 1	Sep. 22	Oct. 12							1.37		**1.37**	
	Lava field area 1	Aug. 31	Oct. 12							58.31	**58.31**		
Phase 2	Lava flow no. 5	Oct. 12	Oct. 28	16	11.71	0.71	0.72	747	811	8.47			
	Lava flow no. 6	Oct. 28	Nov. 19	22	8.45	0.09	1.92	770	811	3.67			
	Lava flow no. 7	Oct. 28	Nov. 19	22	7.11	0.09	1.76	775	811	3.67			
	Lava flow no. 8	Nov. 19	Nov. 30	11	5.42	0.20	1.29	783	811	2.88			
	Flows to the North	Oct. 12	Nov. 30							1.56			
	Inflation plateau 2	Nov. 19	Nov. 30							3.59		**4.96**	
	Resurfacing 2	Nov. 19	Nov. 30							2.39			**2.39**
	Lava field area 2	Oct. 12	Nov. 30							18.70	**77.01**		
Phase 3	Inflation plateau 3	Dec. 1	Feb. 27							13.92		**18.88**	
	In lava flow no. 1	Nov. 19	Dec. 11	22	14.846		0.59			8.74			
	In lava flow no. 2	Dec. 1	Dec. 11	10	11.143		0.78			5.67			
	Lava flow no. 1 + 2	Nov. 19	Dec. 11							14.42			
	Resurfacing 3	Dec. 1	Feb. 27							19.34			**21.73**
	Lava field area 3	Dec. 1	Feb. 27							6.49	**83.50**		

surveillance flights was typically 65°–85° and the distance to the imaged targets was 20–90 km. Hence, the incidence angles created significant shadowing on the far-side of topographic highs. We used amplitude images whose spatial resolution varies from 1 to 12 m/pixel. However, due to the size of the lava field, only limited coverage with 1 m resolution image was obtained. No flight with TF-SIF was carried out between November 14 and until the end of the eruption, but post-eruption data was acquired on April 24, 2015 (Suppl. Table 2).

We also used SAR images acquired by TerraSAR-X (TSX) and COSMO-SkyMed (CSK) satellites to study flow field growth and overall lava morphology. TSX and CSK are both X-band satellites with a right-looking geometry over Iceland. The TSX images were acquired using the StripMap imaging mode, a single polarization (HH) and an incidence angle varying from 22°–45°. The spatial resolution of TSX images is 1.7–3.5 m. The CSK system consists of a constellation of four SAR satellites. We used CSK images acquired in STR-HIMAGE-mode with HH polarization and a view angle range of 23°–32°, providing a spatial resolution of 1.7–3.5 m. Both TSX and CSK data were radiometrically calibrated using the Sentinel-1 toolbox provided by ESA. Refined Lee speckle filtering was applied using a 5 × 5 window, and finally, a Doppler terrain correction was performed using the TanDEM–X intermediate digital elevation model. The airborne SAR data complement the SAR satellite images by providing a higher spatial resolution that resolves detailed internal lava morphologies such as lava channels, boulders, grooves, shear zones and plates. The SAR satellite images, on the other hand, only allow identification of lava channels and other large-scale internal structures.

4. Lava field evolution

Mapping the growth of the lava flow field was enabled by daily to weekly observations during the first two months of activity and then, subsequently, by observations on the time scale of a week from November to February 2015 (Suppl. Table 2).

The flow field evolution has been divided into three main phases based on the dominating type of transport system delivering lava to the active flow fronts (Fig. 2, Table 1).

Phase 1: channel-fed lava transport: August 31 to mid-October
Phase 2: lava ponding: Mid-October to end-November
Phase 3: tube-fed lava transport: Early December to February 27

An overview of lava morphologies mentioned in this section is provided in Suppl. Table 1 and illustrated in Fig. 3 and Suppl. Fig. 1.

4.1. Phase 1: channel-fed lava transport

At the onset of the eruption August 31, 2014 large slabby pāhoehoe sheet flows advanced rapidly from the 1.8 km-long eruptive fissure. Due to radial spreading and cooling of the lava surface, the advance of the flow front slowed down and the flow subsequently began to inflate. These flows were overridden and covered by new sheet flows (Fig. 4A, Suppl. Video 1). As the lava became channelized on September 1 the dominating morphology changed from slabby pāhoehoe to rubbly pāhoehoe and then to ‘a’ā (see e.g. of similar morphological change in Suppl. Fig. 2, Suppl. Table 3, Suppl. Video 2). The lava flow was, in part, controlled by the topography created by the older Holuhraun lavas and by the gentle slope of the flood plain. A large incandescent, and braided, channel system with an area of 0.6 km^2 (15% of the lava flow field at the time; Fig. 5) made up the lava transport system. Individual channels were between 50 and 250 m wide. Over the following couple of days a 6 km-long, open channel developed feeding a 1–2 km wide ‘a’ā flow (Lava flow no.1, Fig. 2, Fig. 4B) that advanced 1–1.5 km/day. The active flow front generally advanced in a conveyor belt-motion, however this pattern was frequently disrupted by a series of 30–50 m-long slabby and rubbly pāhoehoe breakouts from the base of the advancing front (Fig. 4D). These breakouts had initial advance velocities of 30–60 m/h and approached their full length within tens of minutes, then slowed down and inflated for several hours. The

Fig. 2. Overview of the evolution of the 2014–2015 Holuhraun lava field and the dominant lava pathways during the 3 eruption phases. Each color denotes a time period, whereas arrows and hatched lines indicate lava channels and tubes, respectively. (A) During phase 1 (August 31 to mid-October) four flows (No. 1–4) were emplaced. The first indications of lava tube formation were associated with emplacement of flow no. 4 and the inflation plateau close to star #1. (B) Phase 2 (Mid-October 4 to end-November) was dominated by the creation of a lava pond east of the vent (star #2), which becomes the main distributary center for flow no. 5–8. Inflation plateaus in the central part of the lava field indicated that breakouts to the north were tube-fed. (C) In phase 3 (December to February, 27) lava tubes dominated the distributary system. The lava channel from flows no. 1 and 2 had crusted over and inflated, creating elongated lava inflation plateaus, which leaked (primarily from flow no. 2 at star #4) and resurfaced parts of flows no. 1–3. New lobes were emplaced to north. (For interpretation of the references to color in this figure legend, the reader is referred to the web version of this article.)

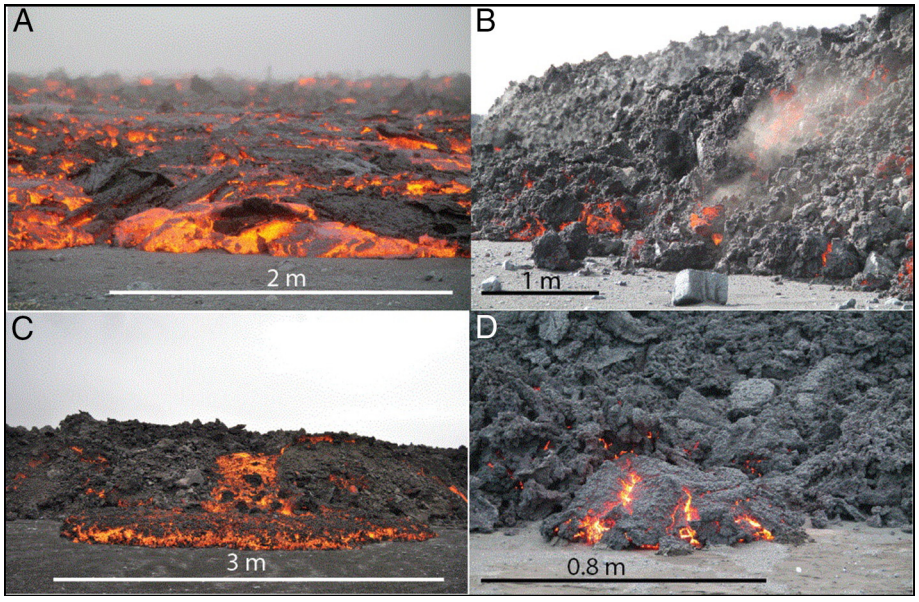

Fig. 3. Four examples of morphologies observed during the 2014–2015 Holuhraun eruption. (A) Slabby pāhoehoe. (B) 'A'ā, (C) Rubbly pāhoehoe. (D) Spiny pāhoehoe. Photo credit: G. B. M. Pedersen (A,B,D) and P. Nikkola (C).

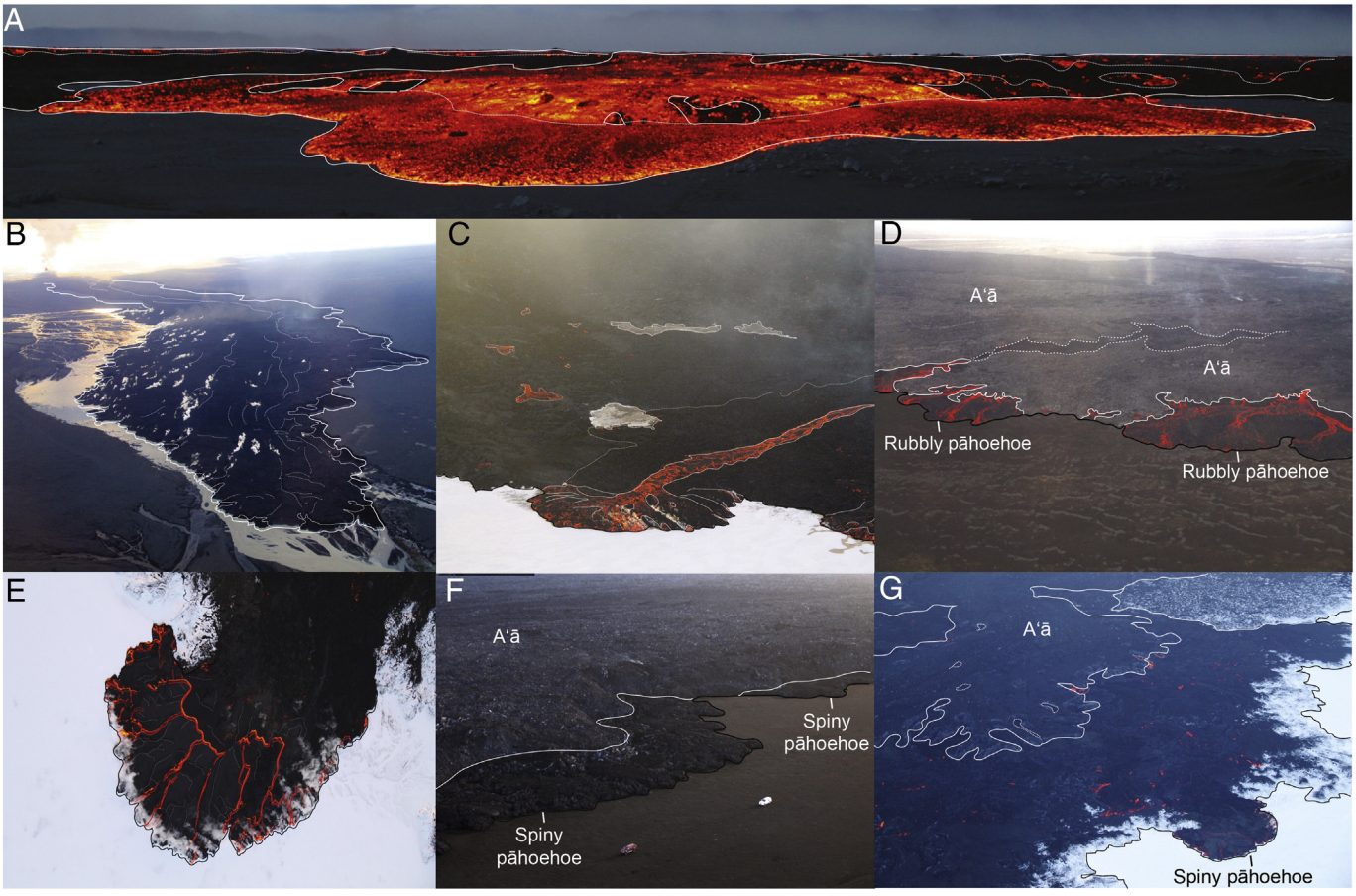

Fig. 4. Examples of active lobe morphology: (A) Slabby pāhoehoe lobe from August 31, 2014 at 20:33. The lobe is approximately 500 m across, (B) 1.8 km wide active 'a'ā flow lobe on September 13, 2014 at 17:36. (C) Emplacement of a ~20 m wide rubbly pāhoehoe lobe on December, 8, 2014 at 12:03. (D) A series of rubbly pāhoehoe lobes along the the front of an advancing 'a'ā flow on September 22, 11:43. (E) Emplacement of a ~20 m wide spiny pāhoehoe lobe on December 8, 2014 at 11:04. (F) Gray 'a'ā flow with small, black, lobes of spiny pāhoehoe along the margin (boundary outlined in white) on September 20 at 16:51. Note the cars for scale. (G) Insulated black, and incandescent, spiny pāhoehoe outbreaks from inflated gray 'a'ā flow. The spiny pāhoehoe field has multiple outbreaks and has been active for a while, hence the older, outer, edge is snow covered (bottom right of the image). The picture is taken on December 8 at 13:30. Photo credit: G. B. M. Pedersen (A, C, E, G), T. Dürig (B, D), and M.T. Gudmundsson (F).

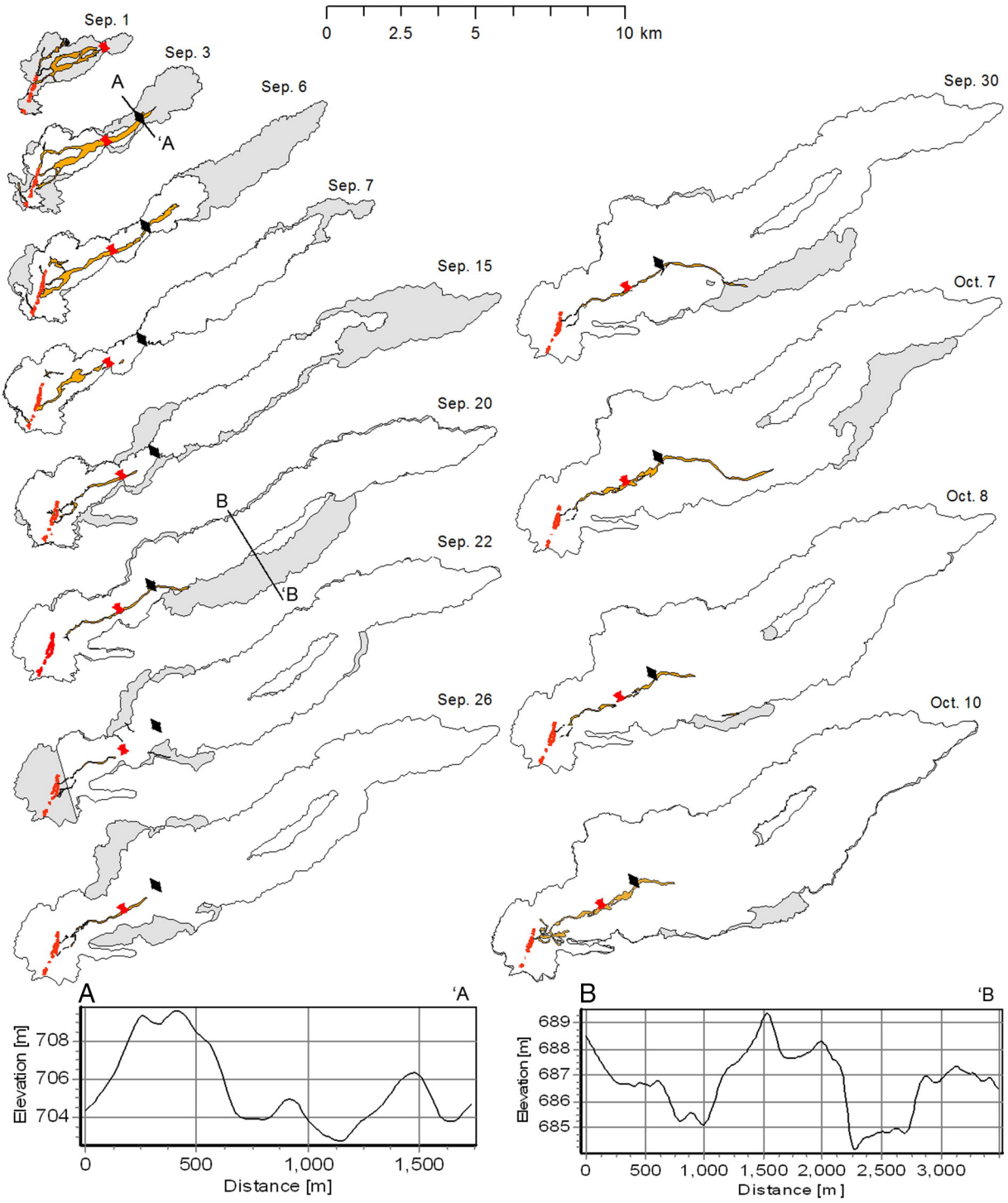

Fig. 5. Lava field development during phase 1. The gray polygon marks the lava outline for the given date, while the white lava outline marks the lava outline for the previous date. Hence the gray area denotes the advancement of lava between those two dates. Note that the white lava outline for September 22 is cut off at the vent area due to the configuration of the satellite flight path. The red line denotes the cone row location and the orange outline marks the lava channel. The red butterfly marks the point where the lava was constricted on September 1 and the black diamond marks the location of constriction on September 3. Profile A-'A shows the pre-eruption topography at the location of constriction on September 3. Profile B-'B shows the pre-eruption topography at the southwestern edge of the kīpuka that formed on September 22. Note the profiles are greatly exaggerated. (For interpretation of the references to color in this figure legend, the reader is referred to the web version of this article.)

breakouts were eventually overrun by the advancing 'a'ā flow front and rarely preserved. A typical example of these short-lived morphological changes from 'a'ā lava to rubbly pāhoehoe within a single lava flows was recorded on September 6 (see Suppl. Video material 2, Suppl. Fig. 3, Suppl. Table 3). Along the lava flow margins, the breakouts were more sporadic, and primarily had the morphology of spiny pāhoehoe and to a lesser degree rubbly to slabby pāhoehoe (Fig. 6).

On September 1 and 3 the sides of the lava flow field were confined by 3–7 m river terraces (Fig. 5). On September 1 the confined channel was only 300 m wide and most likely enforced the development of a single, centralized lava channel, as multiple lava channels originating at different parts of the vent system converged at this location (Fig. 5). On September 3 the point of confinement was 500 m wide and appeared to act as a bottle-neck in the lava pathways which easily got

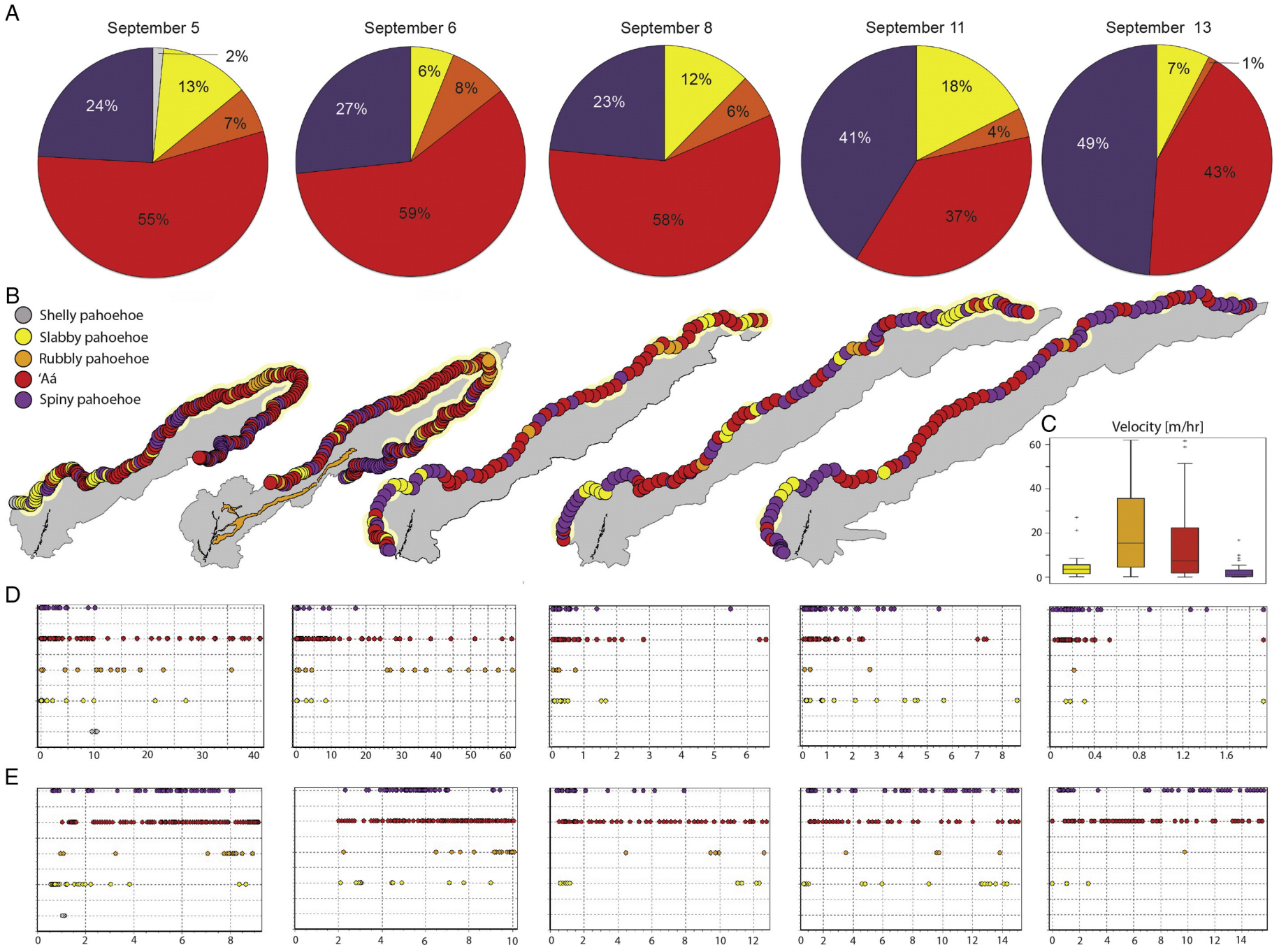
A
September 5
2%
13%
24%
7%
55%
September 6
6%
8%
27%
59%
September 8
12%
23%
6%
58%
September 11
18%
41%
4%
37%
September 13
7%
1%
49%
43%
B
Shelly pahoehoe
Slabby pahoehoe
Rubbly pahoehoe
'Aá
Spiny pahoehoe
C
Velocity [m/hr]
60
40
20
0
D
0 10 20 30 40
0 10 20 30 40 50 60
0 1 2 3 4 5 6
0 1 2 3 4 5 6 7 8
0 0.4 0.8 1.2 1.6
E
0 2 4 6 8
0 2 4 6 8 10
0 2 4 6 8 10 12
0 2 4 6 8 10 12 14
0 2 4 6 8 10 12 14

blocked. Consequently, it became a point of channel divergence affecting the channel development, and hence, influenced the development of the lava flow field throughout the eruption. This location is marked as distributary center 1, and labeled star #1 on Fig. 2. On September 7 the lava flow encountered one of the main branches of the river Jökulsá á Fjöllum, forcing an eastward migration of the river along with passive steaming of the river water (a few steam explosions were observed September 8). Simultaneously, the lava thickened and the maximum flow front velocity was reduced by 90% (Fig. 6D). At the same time the incandescent lava channel shortened from 5.3 km on September 6 to 3.5 km on September 7 (Fig. 5). The first lava flow, no. 1, came to a halt on September 15, 17 km from the vent (Table 1). The dominating morphology of lava flow no. 1 is *'a'ā*, but as the flow slowed down, late-stage breakouts of spiny pāhoehoe were formed along the sides of the flow (Fig. 6). The formation of spiny pāhoehoe took place first along the inactive, central part of the lava flow margins, but as the velocity of the flow front decreased the formation of spiny pāhoehoe were observed along the entire length of the lava flow no. 1 (Fig. 4F, Fig. 6).

Lava flow no. 2 broke out on September 16 at distributary center 1, 4 km from the vent (Fig. 2A, star #1). This flow advanced to the northeast and to begin with and followed the southern margins of lava flow no. 1. At a distance of 7 km from the vent it was diverted southward by a ~5–7 m high mound until it banked up against lava flow no. 1, 11.6 km from the vent. In the process a 3.3 km-long and 0.5 km-wide kīpuka was produced, which survived until mid-December 2014. Thereby the front of lava flow no. 2 came to a halt around September 20, and continued to expand laterally until September 22, widening by 240 m. In the morning of September 21 large channel-fed slabby pāhoehoe outbreaks took place at the northern side of lava flow no. 1. SAR images from the following day (September 22) show that the main channel split close to the distributary center (star #1, Fig. 2A), one to the North and one to the South. This bisection of the channel was visible until September 26, after which lava flow no. 3 began to form, and thereby continued the southeastward lateral progression of the lava flows. Lava flow no. 3 reached its maximum length of 16.3 km on October 7 (Table 1). At that time, it was fed by an 8.2 km-long incandescent lava channel. This lava channel shortened significantly, to 5.6 km, on October 8, when lava flow no. 4 began to form.

During phase 1, the 1.8 km fissure partly closed down and concentrated into a ~500 m long elongated crater with a lava lake in the central part of the fissure, which fed the rest of the eruption. The lava flow field grew 58.3 km^2 and a 1.4 km^2 small inflation plateau developed north of distributary center 1 (star #1, Fig.2A, Table 1).

4.2. Phase 2: lava ponding

Around October 12 lava started ponding 0.8 km east of the vent as a new channel formed as a break out from the previous channel a few hundred meters down from the outlet of the vent. This pond formed on top of the Holuhraun I lava, and between lava flow no. 3 and an earlier 1.7 km long and 250 m wide protruding lobe on the south margin of the 2014 Holuhraun flow field (star #2, Fig. 2B, Fig. 7).

It grew from ca. 0.1 km^2 to 0.9 km^2 in one week and reached maximum area of nearly 1 km^2 on October 28 (Fig. 7). This pond became the primary lava distribution center from mid-October to late November (star #2 on Fig. 2B). After October 28, the pond shrank in size and continued to do so throughout November (Fig. 7) and new outbreaks occurred progressively closer to the lava pond itself. At the same time, the lava flow length decreased from 11.4 km for flow no. 5 to 5.4 km for flow no. 8 (Table 1). Gradually, the pond surface became more packed with plates that accumulated downstream and formed concentric ridges orthogonal to the flow. This lava pond was a persistent feature until the end of the eruption, although it diminished significantly in size after November.

Lava flows no. 5–8 covered 17.6 km^2 (Fig. 2B, Table 1). The aerial SAR images reveal that they have morphologies that resemble those of lava flows no. 1–4. They feature a central channel bounded by levees with well demarcated shear zones, linear grooves formed by flow around obstacles, and sporadic lava ridges orthogonal to the flow direction. In addition to lava flows no. 5–8, a sizable lava lobe (~2.4 km^2) was emplaced on top of lavas from phase 1 and thereby heralded a change from predominantly lateral emplacement to vertical stacking of lava flows.

During phase 2, only minor tube-fed breakouts took place along the northern margins of the lava flow field. In total these breakouts covered 1.6 km^2. Furthermore, satellite SAR images suggest that part of the central channel from lava flow no. 1 was reactivated in mid- November and inflated until late November creating a second 3.6 km^2 inflation plateau within lava flow no. 1 (Fig. 2B, Table 1). This implies that lava tubes became increasingly important for the transport of lava during the end of phase 2.

4.3. Phase 3: tube-fed lava transport

By mid-December inflation plateaus had developed in lava flows no. 1 and 2 (Fig. 2C). This development is revealed by morphological comparisons of airborne SAR images taken November 8, 2014 and April 24, 2015 (Fig. 8). The morphological features within the lava channel, such as the boulders and grooves are preserved, while the surface of the lava channels are elevated with respect to the levees on the April 24 images, creating a stepped cross-flow profile in both lava flows. This demonstrates that the surface of lava channels has been raised by several meters via inflation creating kilometer-long inflation plateaus (Fig. 2C). The inflation plateau in lava flow no. 1 rose between 6 and 10 m above the levees, which were 7–9 m thick, while the inflation plateau in flow no. 2 rose between 5 and 11 m above the levees. Inflation plateaus did not form in lava flows no. 3 to 8.

The inflation plateaus are interpreted to be the surface expression of lava tubes and various field observations confirmed their existence: marginal breakouts with no channel transport system, degassing tracks above lava tubes, inflation clefts, breakouts along the edges of inflation plateaus, small hornitos and tumuli (Suppl. Fig. 4). The levees of lava flow no. 1 are mostly preserved, whereas lavas emplaced in phase 3 resurfaced the levees of lava flow no. 2. By December 11, the elongated kīpuka near the center of the flow field was buried by new lava (Fig. 2C). On December 23, tube-fed breakouts were observed along the northeastern margins of the lava flow field and by mid-January the tube-fed flows reached the far northeast end of the flow, 17.0 km from the vent (Fig. 2C). Thereby, the spiny pāhoehoe breakouts had reached the maximum distance from the vent for the second time, 4 months after lava flow no. 1, which showed 'a'ā morphology.

Along with the breakouts resurfacing the central part of the lava field, new breakouts were observed along the northern margin of the flow field. Some of these started as open channel, fast moving rubbly pāhoehoe lobes that changed to 'a'ā (Suppl. Fig. 2, Suppl. Table 3, Suppl. Video 2) and then changed into spiny pāhoehoe (Fig. 4G). However, most of the outbreaks were lobes of spiny pāhoehoe that were fed by lava tubes that already were established phase 2.

Fig. 6. Temporal distribution of lava morphologies at the margin of lava flow no.1 during the first half of September recorded by using GPS and GoPRO camera. (A) Pie charts show the overall percentage of each lava morphology for each date. (B) The maps show the location of each GoPRO frame, colored according to the main morphology observed at the margin. Occurrence of incandescence is marked with a bright yellow rim. Note that the lava flow went into the river Jökulsá á Fjöllum on September 7 not allowing further access to the southern margin of the flow. North is upward and the maximum length of flow no. 1 is 17 km. (C) Boxplot of the total velocity distribution (m/h) for incandescent lava grouped into lava morphology (number of observations: Slabby pāhoehoe: 18; rubbly pāhoehoe: 27; 'a'ā: 86; spiny pāhoehoe: 34). The box denotes the lower and upper quartiles, and the black line in the middle is the median. The whiskers mark the 1.5 interquartile range. Outliers are plotted as individual points. Note that these velocities are calculated based on 12–24 h time intervals. (D) Diagrams showing the distribution of morphologies with respect to the measured velocity in km/h. (E) Diagrams show the distribution of morphologies with respect to the distance from the vent measured in kilometers. (For interpretation of the references to color in this figure legend, the reader is referred to the web version of this article.)

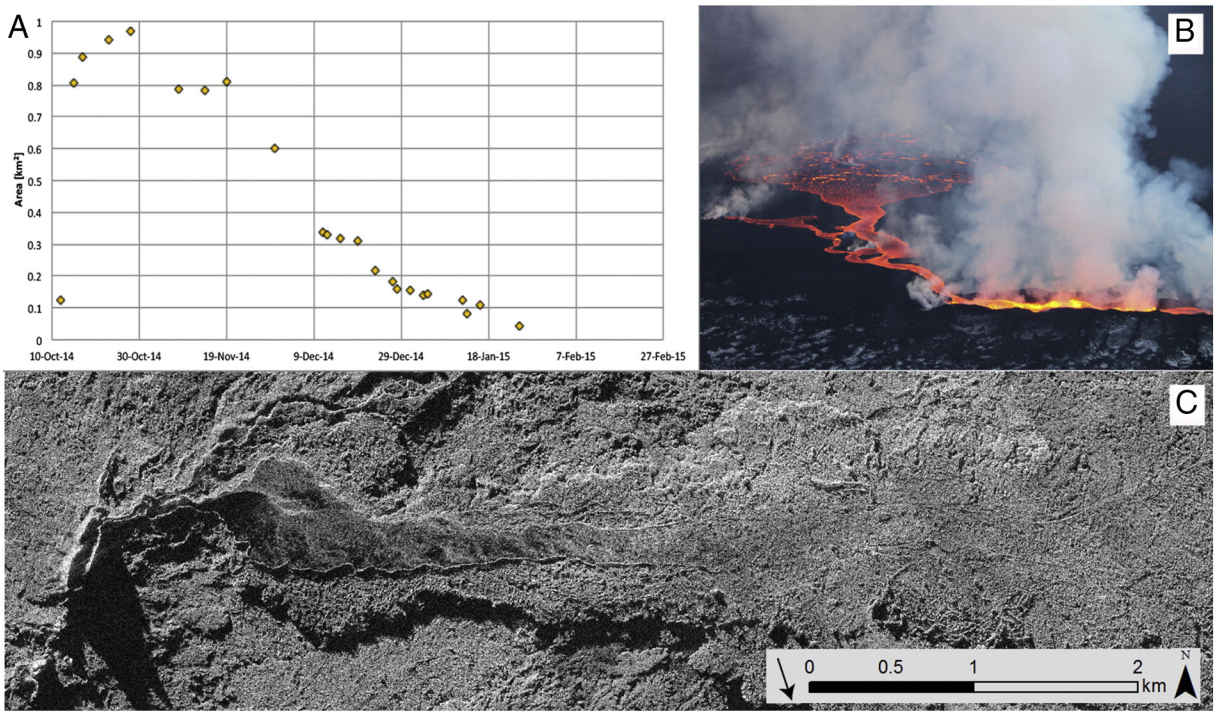

Fig. 7. Lava pond development. (A) The temporal development of the areal (km^2) extent of the pond based on SAR mapping. (B) Photograph of the lava pond with the vent and the lava lake in the foreground. The image is taken December 8, 2014. Photo credit: G. B. M. Pedersen. (C) Aerial SAR-image (3 m/pixel) of the lava pond taken November 8, 2014. The vent and the lava lake can be seen in the left of the image and the crater walls cast a shadow to the southeast because the radar look direction is towards the southeast (shown by the arrow).

The inflation plateaus that formed during phase 3 added 13.9 km^2 to the existing 5.0 km^2 inflation plateaus. An additional 19.3 km^2 of the lava field was resurfaced, and the entire lava field area increased with 5.0 km^2 to 83.5 km^2 (Table 1).

5. Discussion

The 2014–2015 Holuhraun eruption provides an excellent opportunity to study the lava emplacement and the growth of a large lava flow field. During its growth, the lava field changed from being dominated by channels and horizontal expansion, to growth, primarily by inflation, tube-fed flow and vertical stacking of lobes.

5.1. Channel-fed lava transport

The first phase of the eruption is interesting from the perspective of initiation and establishment of the lava transport system. The first 24 h of the eruption were dominated by large, incandescent, slabby pāhoehoe sheet flows spreading rapidly around the active fissure. Over the next 2–3 days one main flow developed (lava flow no. 1), and the lava channel changed from a braided to a single, centralized lava channel.

The incandescent, open-channel fluctuated significantly during emplacement of lava flow no. 1 and no part of the channel could be regarded as the stable channel zone as defined by Lipman and Banks (1987). This may have been partly because the channels close to the vent changed as the eruptive fissure centralized (Fig. 5). It would be more appropriate to term the incandescent channel the transitional channel zone, while the zone downstream could be ascribed to the zone of dispersed flow (Lipman and Banks, 1987; Kilburn and Guest, 1993; Favalli et al., 2010). The incandescent channel shortened significantly September 7 when the lava flow entered the river Jökulsá á Fjöllum. Furthermore, the flow velocities decreased one order of magnitude from September 6 to September 8 and contemporaneously, the lava thickened. The combination of lava thickening and decreased lava front velocity indicates that the river enhanced the cooling sufficiently to increase the yield strength of the lava front, and thus reduced the maximum potential length of the lava flow.

Overflows from the lava channel happened when the lava flow front stalled. These overflow events produced ~50 m wide slabby sheet flows. Unlike the sheet flows in the proximal areas that were overridden from behind (as observed August 31, 2014), these sheet flows were emplaced lobe-by-lobe with repeated inflation and advance cycles (Hon et al., 1994; James et al., 2015) and can be regarded as sheet lobes (Self et al., 1998). Most of the slabby pāhoehoe sheet flows in phase 1 are not exposed at the surface because later lavas covered them. Hence, Holuhraun illustrates that studies of long-lived eruptions based on surface morphology (e.g. Rossi, 1996) may be unable to observe the morphological evidence of episodes with high-effusion rate, which will bias the results towards lower effusion rate scenarios.

5.2. Lava ponding

The lava pond formed quickly over a 2–3-day period during emplacement of lava flow no. 5 (Fig. 7). The timing of the development of

Fig. 8. Formation of inflation plateaus. (A1 and B1) Sections of lava flow no. 1 and 2 imaged by airborne SAR November 8, 2014. The red arrows show boulders and grooves within the lava flow and the black arrow shows the radar look direction. The locations of these sections are highlighted with black boxes on the inset map of the 2014–2015 Holuhraun lava field from phase 2 (similar to Fig. 2B). (A2 and B2) The same sections of lava flow no. 1 and 2 imaged by airborne SAR April 24, 2015. The boulders and grooves seen in A1 and B1 are preserved but the flows reveal a step-wise topography. The lava channels have inflated forming the inflation plateaus, which casting the visible dark shadows to the northwest, while the surrounding margins are lower. In B2 the levees of lava flow no. 2 has been partly resurfaced. The inset maps show the 2014–2015 Holuhraun lava field from phase 3, where inflation plateaus are mapped in light gray (similar to Fig. 2C). (C1) Sketch illustrating A1 and B1 as a lava flow with boulders, shear zones and grooves. A fluid core exists within the lava channel under the channel roof. (C2) The lava flow became re-activated and the fluid core acted as a flow path for new lava inflating the lava channel and thereby forming the inflation plateau. This illustrates A2. (C3) When the inflation of the channel continues, the roof eventually breaks and new breakouts leek from the edges of the inflation plateau and resurface the levees of the lava flow. This illustrates B2. (For interpretation of the references to color in this figure legend, the reader is referred to the web version of this article.)

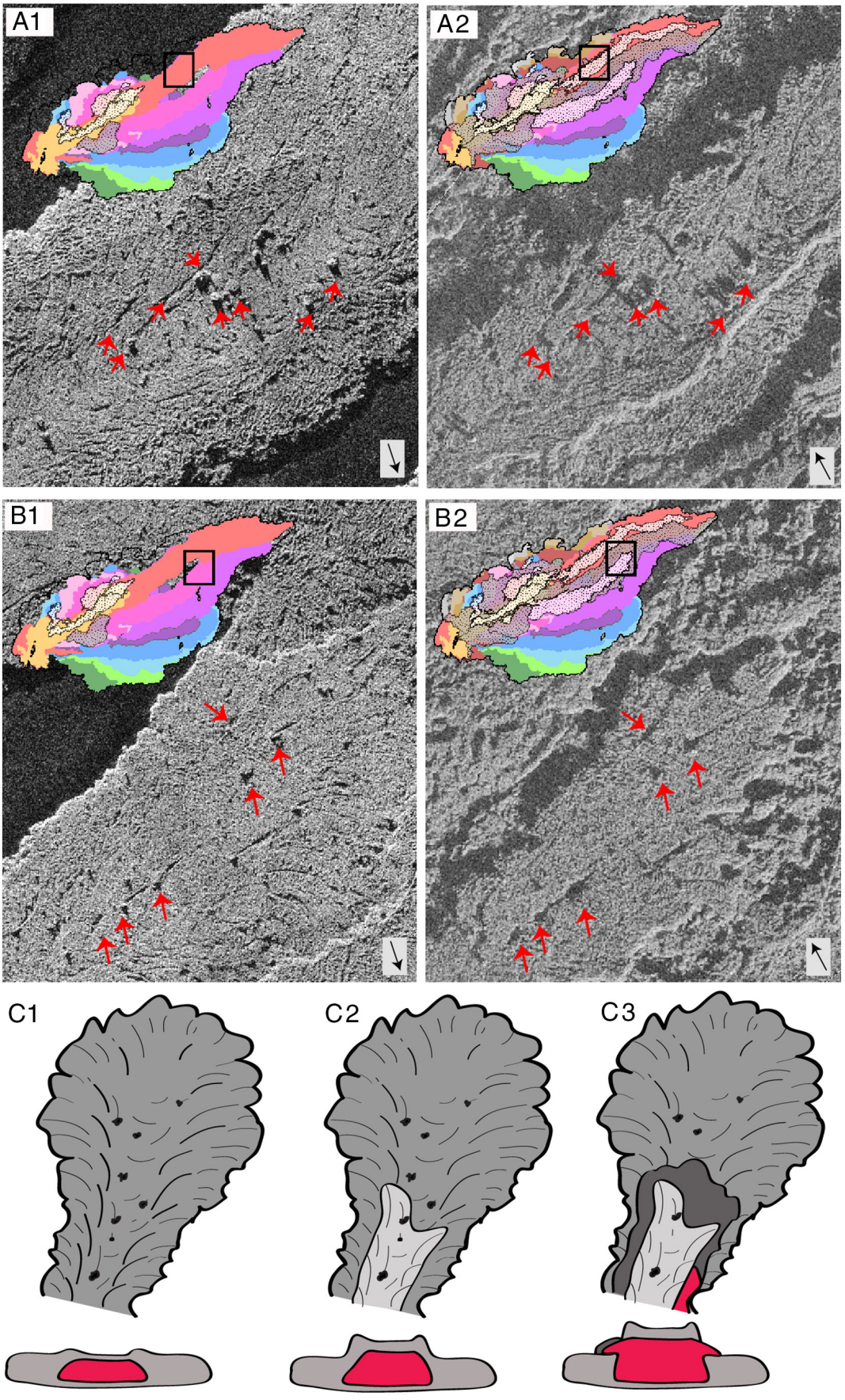
A1
A2
B1
B2
C1
C2
C3

the pond is preceded by a break out from the open channel close to the active vent, probably due to clogging, which caused a southward migration of the lava field (Fig. 2). The formation of the pond in lava flow no. 5 is likely to be linked to the pre-emplacement topography. The profiles of the pre-eruptive topography of the substrate for the eight lava flows reveal that the center lines of the first two lava flows had a fairly smooth decrease in elevation from source to lava front (Suppl. Fig. 5). Lava flows no. 3 to 5 had a few bigger obstacles along their profiles, whereas lava flows no. 6 to 8 had increase in elevation for 0.5–1 km at their far ends (Suppl. Fig. 5). As a result, flows no. 6 to 8 began to stall, which explains why these flows are short, wide, and advanced slowly (Table 1, Fig. 9). This suggests that the channel system was full of molten lava from source to front allowing the flow front to inflate sufficiently to advance 5–8 m uphill.

Thus, we propose that the growth of the lava pond was a result of resistance from the bounding lava field envelope and partly due to the rising topography towards the south.

The residence time within the lava pond must have been short because the pond was bubbling and not able to crust over until the month of February. Furthermore, we also conclude that the lava pond may, to a minor degree, have worked as a local storage for the lava that was distributed into lava tubes, which were developed throughout November and into December.

5.3. Tube-fed lava transport

Lava tubes in 'a'ā flows have been observed previously during Etna eruptions, but their formation and development is not fully understood (e.g. Guest et al., 1987; Calvari and Pinkerton, 1998).

The inflation plateaus are interpreted as the surface manifestation of lava tubes and they provide remarkable information on lava tube formation in 'a'ā flows. First, of all, they are evidence of month-long interconnection of the lava pathways within the lava field. Secondly, this inflation is tightly connected to the lava flow channels that formed during the initial emplacement. Thirdly, formation of lava tubes may occur several months after the emplacement of the 'a'ā flows themselves. Finally, the tubes are very important as they controlled the distribution of lava in phase 3, and therefore, mark the change in emplacement dynamics from lateral spreading to re-surfacing.

The inflation plateaus developed gradually in phase 2 and 3 and the two-step topography observed in lava flow no. 1 and 2, suggests that the new lava pathway was confined to the channel, between the channel roof and the base of the flow (Fig. 8). The exact origin of this pathway within the lava flow is unknown based on our data. Either (a) the lavastatic pressure in the fluid core caused by upstream lava ponding was sufficient to lift the channel roof creating space for new lava, or (b) the lava initially migrated along cavities below the channel roof, which could have formed by e.g. drainage of the lava core and/or contraction of lava due to cooling. Subsequently the lavastatic pressure within this new lava increased due to damming of lava upstream and subsequently lifted the channel roof.

The fact that the inflation plateaus only are observed in lava flow no. 1 and 2 is intriguing (Fig. 2). If the origin of the pathway was caused by (a) the two-step topography, could be explained by disconnection of the fluid lava in the channel and the levees. Therefore the inflation only occurred within the lava channel in lava flow no. 1–2. The lack of observed inflation plateaus in flows no. 3 to 8 may then either suggest that the lavastatic pressure in these lava channels did not increase

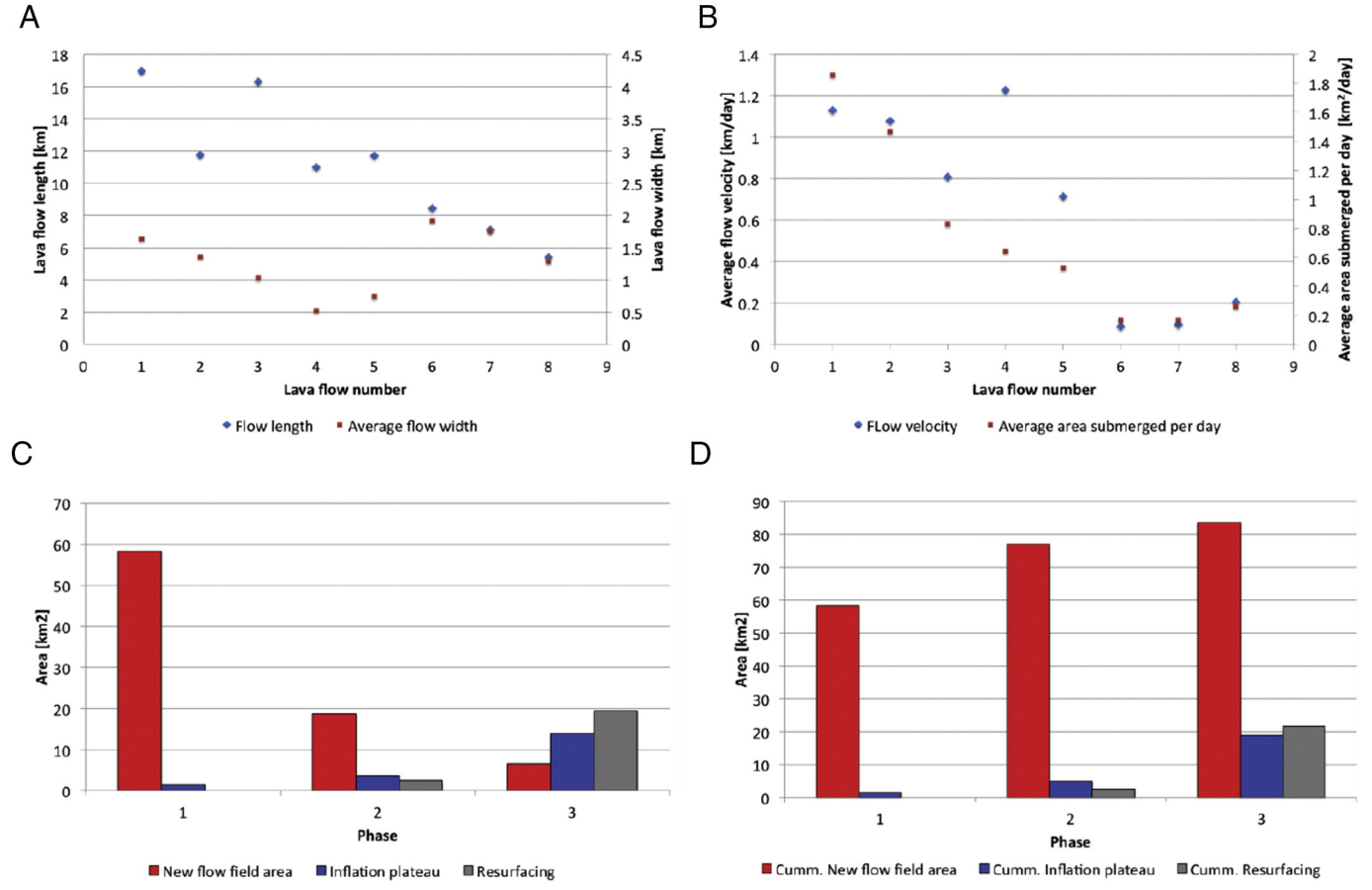

Fig. 9. (A) Length and width of lava flow no. 1 to 8. (B) Average flow velocity and average area submerged per day for lava flow no. 1 to 8. (C) Overview of the new flow field area, inflation area and resurfaced area for each of the 3 eruption phases. (D) Overview of the cumulative flow field area, cumulative inflation area and cumulative resurfaced area during the eruption phases.

sufficiently or that the inflation in these lava flows was broader and not confined to the lava channel. This unconfined inflation did not create a two-step-topography as seen in lava flow 1–2, and can therefore not be revealed by SAR imagery. If the origin of the pathway was caused by (b) the fact that the two-step topography only is observed in lava flow no. 1–2 could be explained by cavities only existing in lava flow no. 1–2 and not lava flow no. 3–8.

The question is why the lava tube transport became dominant in the end of November- beginning of December. The emplacement of lava flows no. 6–8, was limited because of the rising topography towards the south. Hence, the lava flows no. 6–8 were both cooling and topographically limited, whereas lava flow no. 1 and 3 to 5 were cooling limited. Lava flow no. 2 banked up against lava flow no. 1, and could potentially have advanced further, since its length is 4.5 km shorter than lava flow no. 3, which most likely was emplaced during similar or lower discharge rates. Consequently, the discharge-capacity of the southern lava pathways related to the distributary center #2 was not sufficient, and as a result two lava flows progressively developed to the north. Apparently, neither of these changes accommodated all the lava discharged at the vent and inflation took place within the lava channel of lava flow no. 1 creating an inflation plateau from 1 km to 6.9 km from the vent (Fig. 2B).

If we assume that the uplift of the channel roof was elastic, and friction free, an inflation plateau of 5–10 m height could form after the open channel had built up a minimum height of 5–10 m above the fluid lava under the channel roof. This would cause the lavastatic pressure to be equal to the lithostatic load pressure of an inflation plateau of 5–10 m. For 1 m^2 of the lava channel roof (with a density of ~2300 kg/m^3) the resultant lithostatic load would be in the range of 110–225 kPa. Though the formation of the tubes was not friction free, these numbers are a very modest, and we therefore find that it is reasonable to assume that the topographic barriers, induced by the surroundings and the lava field itself, dammed sufficient lava in the open channel system.

In order to uplift the inflation plateau in flow no. 1 by 5–10 m, 0.04–0.09 km^3 new lava was required. An additional 0.03–0.06 km^3 lava was required to uplift the inflation plateau in flow no. 2 (Table 1). The total inflation area is 18.9 km^2, and if the uplift is of the same range, this requires a total volume of 0.09 km^3 to 0.18 km^3.

5.4. Evolution of lava morphology

Major changes in surface morphology of the lava took place several times during the three phases of 2014–2015 eruption. The first major change took place within the first days of the eruption, when slabby pāhoehoe sheet flows changed into rubbly pāhoehoe and then into a'ā downstream. These changes are very similar to typical morphological transitions described previously (Lipman and Banks, 1987; Cashman et al., 1999; Hon et al., 2003).

Short-lived morphological changes from a'ā lava to rubbly pāhoehoe to a'ā were observed multiple times at the active flow front of the large a'ā flows during their emplacement in phase 1–2 (Fig. 3F, Suppl. Video material 2, Suppl. Fig. 3, Suppl. Table 3). During these changes the a'ā lobe progressively changed character from being one tall lobe to consist of a couple of less tall, but more incandescent a'ā lobes, which then eventually would feed breakouts of rubbly pāhoehoe. The fact that these changes happened gradually, that they happened multiple times and that no changes in feeding system upstream was observed suggest that these short-lived morphological changes were a part of the emplacement dynamics of the a'ā flow itself. These short-lived morphological changes from a'ā to rubbly pāhoehoe were changes in morphology along a single flow and were generally occurring at the front of advancing lobes. However, the change in the morphology did not mark a permanent change from a'ā to rubbly pāhoehoe downflow and we therefore denote these morphological changes short-lived transitions.

The morphology of the late-stage breakouts along the margins of the stalling a'ā flows was typically spiny pāhoehoe. These observations are similar to previous observations of toothpaste lava and slab-crusted lava (displaying very similar properties to spiny pāhoehoe) that often occur at distal ends of pāhoehoe (Rowland and Walker, 1987) or as late-stage breakouts from inflating ‘a’ā flows (Camp et al., 1987; Jurado-Chichay and Rowland, 1995; Rossi, 1997; Guest and Stofan, 2004).

In phase 1–2 the spiny pāhoehoe breakouts stopped after a short while (Fig. 3E), as new a'ā flows were emplaced elsewhere. However, in phase 3 it was observed that this mode of spiny pāhoehoe emplacement continued and marked a permanent change in flow morphology (Fig. 3G).

The above mentioned continuous development of morphologies suggest that there is evolutionary continuum of morphologies from slabby pāhoehoe to rubbly pāhoehoe to a'ā as previously alluded to by Thordarson and Sigmarsson (2009) for the lava flows of the 1963–67 Surtsey eruption of the south coast of Iceland. The transformation from a'ā to spiny pāhoehoe, suggest that the morphological continuum should be expanded to include spiny pāhoehoe. The evolution of morphologies during the emplacement of the 2014–2015 Holuhraun lavas is visualized in Fig. 10. In phase 1–2 the dominating morphology was ‘a’ā while spiny pahoehoe was dominating in phase 3. This change in morphology from mainly ‘a’ā in phase 1–2 and spiny pāhoehoe in phase 3 makes Holuhraun a paired lava field. Paired flow fields have been suggested to form due to the decline of effusion rate over the course of an eruption (Rowland and Walker, 1990). Hence, ‘a’ā would form during the high effusion phase and pāhoehoe would form during low effusion rate. Interestingly, it has been noted that within many Hawaiian paired flows both flow morphologies reach a similar length (Rowland and Walker, 1990). Based on the observations at Holuhraun, we suggest that the similar length can arise from the fact that the pāhoehoe is fed from the tube system utilizing the existing ‘a’ā lava channels, and thereby controlled by the initial length of the ‘a’ā flows. Hence, paired flows will be prone to have similar lengths unless new tube systems develop.

The Holuhraun lava was emplaced onto a near-flat floodplain and the chemical composition of the lava is uniform throughout the whole eruption (Gislason et al., 2015; Thordarson et al., 2015; Gudmundsson et al., 2016). This implies that neither the topography nor the composition were the driving factors for the observed changes in flow morphology. The first transition of slabby pāhoehoe to rubbly pāhoehoe to a'ā occurred downstream of the vent, consistent with such changes in other lava producing eruptions and are explained by increased viscosity due to stirring, cooling and gas loss during lava transport (e.g. Macdonald, 1953; Cashman et al., 1999 and Hon et al., 2003).

However, the short-lived transitions from ‘a’ā to rubbly pāhoehoe back to ‘a’ā demonstrates that the lava enveloped by the ‘a’ā crust could retain its heat via insulation. This allowed the active ‘a’ā lava flow to retain a low viscosity core that upon breakout created different surface morphologies than ‘a’ā (e.g., Guest, 1982; Guest et al., 1987; Calvari and Pinkerton, 1999; Hon et al., 2003; Guest and Stofan, 2004). Likewise, spiny pāhoehoe breakouts clearly originated from the a'ā flow and may either imply (i) the presence of a fluid lava within the interior of the a'ā flow (yet viscous enough to form spiny pāhoehoe) or (ii) a change in strain rate caused by the decrease in flow velocity.

The distribution of observed morphology was much more complex than a simple correlation to vent distance and our observations show that the maximum flow velocity measured during emplacement was correlated to morphology (Suppl. Table 1, Fig. 6c). As documented the slabby pāhoehoe had flow velocities of 800–1000 m/h followed by rubbly pāhoehoe and ‘a’ā, which had flow velocities up to 65 m/h. The spiny pāhoehoe had the lowest observed flow velocities of 1–4 m/h (Suppl. Table 1). This suggests that the lava flow velocity and thus the local lava flux had a strong influence on the crust

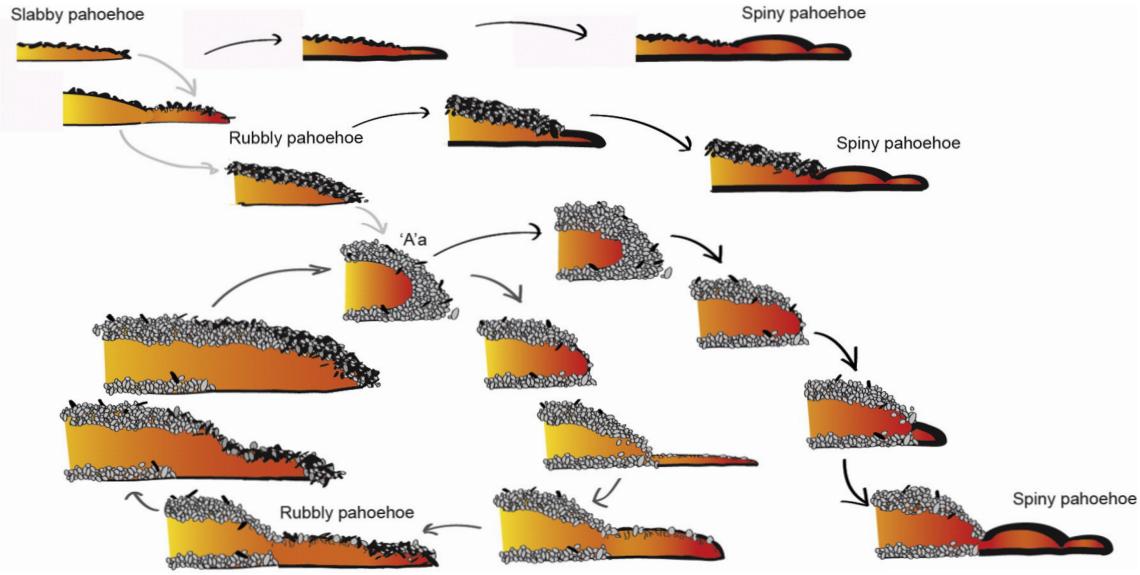

Fig. 10. Sketch of morphological evolution of the 2014–2015 Holuhraun lava field. Initially the slabby pāhoehoe lobes developed and transitioned into rubbly pāhoehoe and 'a'ā. During phase 1–2, when large 'a'ā lava flows were emplaced (lava flow no. 1–8), the frontal morphology changed from 'a'ā to rubbly pāhoehoe and back to 'a'ā. These changes were short-lived but observed repeatedly and have therefore drawn as cycle. Often, after an 'a'ā flow stopped, spiny pāhoehoe lobes were emplaced at the margin of the flow. During continued low-discharge lava supply, breakouts can continue as spiny pāhoehoe converting the lava field from 'a'ā upstream to spiny pāhoehoe downstream. Change from rubbly and slabby pāhoehoe to spiny pāhoehoe was also observed, although only to a minor extent.

formation and thereby on the lava morphology. Hence, the distribution of the lava morphologies is connected to the evolution of the entire lava field, which can develop different local conditions at any given place within the field. This is because a sizable lava field like Holuhraun is able to insulate and store molten lava in localized areas. Thereby a parameter such as vent distance is buffered by the size and distribution of these local storage zones within the lava field. The vent distance does not reveal the complexity of the lava cooling history, which is controlled determined by the 'local' lava flux, the length lava pathway, and the mode of lava emplacement (Hon et al., 2003). However, an overall decrease in effusion rate will eventually lead to decrease in local lava flux and flow velocity and thus cause a change in morphology. Hence a decrease in effusion rate can explain the change from 'a'ā dominant morphology in phase 1–2 to spiny pāhoehoe in the three phase.

6. Conclusions

The 6-month long eruption at Holuhraun 2014–2015 was the largest effusive eruption in Iceland in 230 years with an estimated bulk lava volume of ~1.44 km^3. The eruption has been divided into three phases based on the lava field evolution. The first phase was dominated by open lava channels and emplacement of lava flows no. 1–4. The lava flows were predominantly cooling limited and the longest is lava flow no. 1, which reached the length of 17 km. Lava emplacement during the second phase was influenced by the formation of a 1 km^2 lava pond about 1 km downstream of the vent. This pond became the main distribution point for the lava during phase 2, controlling the emplacement of lava flows no. 5–8. Towards the end of phase 2 vertical stacking of lava lobes became more predominant and lava tubes developed within the channel system of lava flow no. 1, resulting in formation of inflation plateaus. In the third and final phase, transport of lava through tubes continued and inflation plateaus grew in extent, both in lava flows no. 1–2, raising the original channel surface by 5–10 m above the surrounding lava. >19 km^2 of the lava field was resurfaced during this period, and lavas were emplaced in the distal end of the lava flow field. We suggest that the topography (both of the surroundings and of the lava field itself) made it possible to build up the open channel system so it minimum was 5–10 m higher than the fluid lava in flow no. 1–2. This damming increased the lavastatic pressure in the lava, which was sufficient to lift the roof of the lava channels creating the inflation plateaus, allowing new lava to be transported to the distal ends of the lava field.

A suite of lava morphologies (shelly pāhoehoe, slabby pāhoehoe, rubbly pāhoehoe, spiny pāhoehoe and 'a'ā) was observed within the first week of the eruption. During phase 1 and 2 'a'ā was the dominant flow morphology of lava flows no. 1–8 and in phase 3 spiny pāhoehoe was the typifying lava morphology. These changes in surface morphology makes the 2014–2015 Holuhraun lava a paired flow field and the development of lava tubes along existing channels within the 'a'ā flow may explain why paired lava flows often have similar length. Finally, the 2014–2015 Holuhraun eruption illustrates that it is likely that the initial products of the high-effusion phase will not be visible in long-lived eruptions, biasing analysis of surface morphologies of lavas towards lower effusion rate scenarios.

Supplementary data to this article can be found online at http://dx.doi.org/10.1016/j.jvolgeores.2017.02.027.

Acknowledgements

The authors would like to thank everybody who contributed to the data collection in the field, and a special thanks go to Sveinbjörn Steinþórsson and Þorsteinn Jónsson for their invaluable technical support. Furthermore, we thank Morgan Jones for proofreading of the manuscript. Extended thanks goes to the staff at the Icelandic Coast Guard who collected the airborne SAR imagery and provided helicopter support. The COSMO-SkyMed data were provided by the Italian Space Agency (ASI) and TerraSAR-X data by the German Space Agency (DLR) through the Icelandic Volcanoes Supersite project supported by the Committee on Earth Observing Satellites (CEOS). Furthermore, an intermediate TanDEM-X digital elevation model was provided by DLR under project IDEM_GEOL0123. The LANDSAT image was made available by the U.S. Geological Survey. The work was financed with crisis response funding from the Icelandic Government along with European Community's Seventh Framework Programme Grant No. 308377 (Project FUTUREVOLC) and along with the Icelandic Research fund, Rannis, Grant of Excellence No. 152266-052 (Project EMMIRS). Furthermore, Vinur Vatnajökuls are thanked for support.

References

Ágústdóttir, T., Woods, J., Greenfield, T., Green, R.G., White, R.S., Winder, T., Brandsdóttir, B., Steinthórsson, S., Soosalu, H., 2016. Strike-slip Faulting During the 2014 Bárðarbunga-Holuhraun Dike Intrusion, Central Iceland. GRL. http://dx.doi.org/10.1002/2015GL067423.

Calvari, S., Pinkerton, H., 1998. Formation of lava tubes and extensive flow field during the 1991–1993 eruption of Mount Etna. J. Geophys. Res. 103 (Bll, 27), 291–27,301.

Calvari, S., Pinkerton, H., 1999. Lava tube morphology on Etna and evidence for lava flow emplacement mechanisms. J. Geophys. Res. 90 (3–4), 263–280.

Camp, V.E., Hooper, P.R., Roobol, M.J., White, D.L., 1987. The Madinah eruption, Saudi Arabia: magma mixing and simultaneous extrusion of three basaltic chemical types. Bull. Volcanol. 49, 489–508.

Cashman, K.V., Thornber, C., Kauahikaua, J.P., 1999. Cooling and crystallization of lava in open channels, and the transition of Pāhoehoe Lava to 'A'ā. Bull. Volcanol. 61, 306–323.

Coppola, D., Ripepe, M., Laiolo, M., Cigolini, C., 2017. Modelling Satellite-derived magma disharge to explain caldera collapse. Geology. http://dx.doi.org/10.1130/G38866.1.

Eibl, E.P.S., Christopher, J.B., Vogfjörd, K.S., Ying, Y., Lokmer, I., Möllhoff, M., O'Brien, G.S., Pálsson, F., 2017. Tremor-rich shallow dyke formation followed by silent magma flow at Bárdarbunga in Iceland. Nat. Geosci.

Einarsson, P., Sæmundsson, K., 1987. Earthquake epicenters 1982–1985 and volcanic systems in Iceland (map). In: Sigfússon, Þ.I. (Ed.), Í hlutarins eðli, Festschrift for Þorbjörn Sigurgeirsson. Menningarsjóður, Reykjavík.

Favalli, M., Harris, A.J.L., Fornaciai, A., Pareschi, M.T., Mazzarini, F., 2010. The distal segment of Etna's 2001 basaltic lava flow. Bull. Volcanol. 72:119–127. http://dx.doi.org/10.1007/s00445-009-0300-z.

Gislason, et al., 2015. Environmental pressure from the 2014–15 eruption of Bárdarbunga 212 volcano, Iceland. Geochem. Persp. Let. 1, 84–93.

Gudmundsson, et al., 2016. Gradual caldera collapse at Bárdarbunga volcano, Iceland, regulated by lateral magma outflow. Science:353, aaf8988. http://dx.doi.org/10.1126/science.aaf8988.

Guest, J.E., 1982. Styles of eruption and flow morphology on Mt. Etna. Mem. Soc. Geol. Ital. 23, 49–73.

Guest, J.E., Stofan, E.R., 2004. The significance of slab-crusted lava flows for understanding controls on flow emplacement at Mount Etna, Sicily. J. Volcanol. Geotherm. Res. 142, 193–205.

Guest, J.E., Kilburn, C.R.J., Pinkerton, H., Duncan, A.M., 1987. The evolution of lava flow-fields: observations of the 198 and 1983 eruptions of Mount Etna, Sicily. Bull. Volcanol. 49, 527–540.

Guilbaud, M., Self, S., Thordarson, T., Blake, S., 2005. Morphology, surface structures, and emplacement of lavas produced by Laki, A.D. 1783–1784. Geol. Soc. Am. Spec. Pap. 396:81–102. http://dx.doi.org/10.1130/0-8137-2396-5.81.

Harris, A.J.L., Rowland, S.K., 2015. Lava flows and rheology. In: Sigurdsson, H., Houghton, B., McNutt, S.R., Rymer, H., Stix, J. (Eds.), Encyclopedia of Volcanoes. Academic Press, USA.

Harris, A.J.L., Rowland, S.K., Villeneuve, N., Thordarson, T., 2017. Pāhoehoe, 'a'ā, and block lava: an illustrated history of the nomenclature. Bull. Volcanol. 79:7. http://dx.doi.org/10.1007/s00445-016-1075-7.

Hartley, M.E., Thordarson, T., 2013. The 1874–1876 volcano-tectonic episode at Askja, North Iceland: lateral flow revisited. Geochem. Geophys. Geosyst. http://dx.doi.org/10.1002/ggge.20151.

Hjartardóttir, Á.R., Einarsson, P., Magnúsdóttir, S., Björmsdóttir, Þ., Brandsdóttir, B., 2015. Fracture systems of the Northern Volcanic Rift Zone, Iceland: an onshore part of the Mid-Atlantic plate boundary. In: Wright, T.J., Ayele, A., Ferguson, D.J., Kidane, T., Vye-Brown, C. (Eds.), Magmatic Rifting and Active Volcanism. London, Special Publications, Geological Society:p. 420. http://dx.doi.org/10.1144/SP420.1.

Hjartardóttir, Á.R., Einarsson, P., Gudmundsson, M.T., Högnadóttir, T., 2016. Fracture movements and graben subsidence during the 2014 Bárðarbunga dike intrusion in Iceland. J. Volcanol. Geotherm. Res. 310, 242–252.

Hon, K., Kauahikaua, J., Denlinger, R., Mackay, K., 1994. Emplacement and inflation of pahoehoe sheet flows: observations and measurements of active lava flows on Kilauea volcano, Hawaii. Geol. Soc. Am. Bull. 106 (3), 351–370.

Hon, K., Gansecki, C., Kauahikaua, J., 2003. The transition from 'A'ā to Pāhoehoe crust on flows emplaced during the Pu'u 'Ō'ō-Küpaianaha eruption. In: Heliker, C.C., Swanson, D.A., Takahashi, T.J. (Eds.), The Pu'u 'Ō'ō-Küpaianaha Eruption of Kilauea Volcano, Hawai'i: The First 20 Years. USGS Prof Paper 1676, pp. 89–103.

Höskuldsson, A., Óskarsson, N., Pedersen, R., Grönvold, K., Vogfjörð, K., Ólafsdóttir, R., 2007. The millennium eruption in Hekla in February 2000. Bull. Volcanol. 70, 169–182.

Höskuldsson, A., Jónsdóttir, I., Riishus, M.S., Pedersen, G.B.M., Gudmundsson, M.T., Thordarson, T., Drouin, V., the Futurevolc IES field work team, 2015. Magma Discharge and Lava Field Growth in the Nornahraun/Bardabunga Eruption in Iceland. European Geosciences Union, General Assembly. vol. 17 p. 10753 (Vienna, Austria).

Höskuldsson, A., Jónsdóttir, I., Thordarson, T., 2016. Futurevolc and the Bardarbunga Eruption 2014–15 Iceland, Success in the Field and Laboratory. European Geosciences Union, General Assembly. vol. 18 p. 13687 (Vienna, Austria).

James, M.R., Tuffen, H., Hancock, A., Höskuldsson, A., Thórðarson, T., Guðmundsson, M.T., Pedersen, G.B.M., Riishuus, M.S., 2015. Growth of the Holuhraun Lava Flow by Sequential Lobe Emplacement, as Quantified by Time-lapse Terrestrial Lidar Measurements. 26th IUGG, VS02p-450,Prague, Czech Republic.

Johannesson, H., Sæmundsson, K., 1998. Geological Map of Iceland, 1: 500,000. first ed. Höggun. Icelandic Institute of Natural History, Reykjavik, Iceland.

Jónsdóttir, I., Thordarson, T., Höskuldsson, A., Sæmundsson, Þ., 2014. Real-time monitoring of volcanic eruptions in Iceland 2004–2014 using satellite images. Jökull 29, 7–28.

Jurado-Chichay, Z., Rowland, S.K., 1995. Channel overflows of the Pōhue Bay flow, Mauna Loa, Hawai'i: examples of the contrast between surface and interior lava. Bull. Volcanol. 57:117. http://dx.doi.org/10.1007/BF00301402.

Keszthelyi, L., McEwen, A.S., Thordarson, T., 2000. Terrestrial analogs and thermal models for Martian flood lavas. J. Geophys. Res. 105 (E6):15,027–15,049. http://dx.doi.org/10.1029/1999JE001191.

Keszthelyi, L., Thordarson, T., McEwen, A., Haack, H., Guilbaud, M., Self, S., Rossi, M.J., 2004. Icelandic analogs to Martian flood lavas. Geochem. Geophys. Geosyst. 5:Q11,014. http://dx.doi.org/10.1029/2004GC000758.

Kilburn, C.R., 1981. Pahoehoe and aa lavas: a discussion and continuation of the model of Peterson and Tilling. J. Volcanol. Geotherm. Res. 11, 373–382.

Kilburn, C.R., Guest, J.E., 1993. Aa lavas of Mount Etna, Sicily. In: Kilburn, C.R.J., Luongo, G. (Eds.), Active Lavas: Monitoring and Modelling. UCL Press, London, Ch, p. 3.

Larsen, G., Gudmundsson, M.T., Vogfjörð, K., Ilyinskaya, E., Oddsson, B., Pagneux, E., 2015. The Bárðarbunga volcanic system. In: Ilyinskaya, Larsen, Gudmundsson (Eds.), Catalogue of Icelandic Volcanoes. IMO, UI, CPD-NCIP.

Lipman, P.W., Banks, N.G., 1987. Aa Flow Dynamics, Mauna Loa. USGS Prof Pap 1350. pp. 1527–1567.

Macdonald, G.A., 1953. Pahoehoe, aa, and block lava. Am. J. Sci. 251 (3), 169–191.

Óladóttir, B.A., Larsen, G., Sigmarsson, O., 2011. Holocene volcanic activity at Grímsvötn, Bárdarbunga and Kverkfjöll subglacial centres beneath Vatnajökull, Iceland. Bull. Volcanol. 73:1187. http://dx.doi.org/10.1007/s00445-011-0461-4.

Pedersen, G.B.M., Höskuldsson, A., Riishuus, M., Jónsdóttir, I., Gudmundsson, M.T., Sigmundsson, F., Óskarsson, B.V., Dürig, T., Drouin, V.J.P.B., Gallagher, C., Askew, R., Moreland, W.M., Dumont, S., Davies, A., Keszthelyi, L., Hamilton, C.W., Thordarson, T., 2015. Nornahraun lava morphology and emplacement: a new terrestrial analogue for planetary lava flows. 46th LPSC, The Woodlands, Texas, USA.

Peterson, D.W., Tilling, R.I., 1980. Transition of basaltic lava from pahoehoe to aa, Kilauea Volcano, Hawaii: field observations and key factors. J. Volcanol. Geotherm. Res. 7 (3–4), 271–293.

Reynolds, H.I., Gudmundsson, M.T., Högnadóttir, T., 2015. Subglacial Melting Associated With Activity at Bárðarbunga Volcano, Iceland, Explored Using Numerical Reservoir Simulations. European Geosciences Union, General Assembly 2015. vol. 17 p. 10753 (Vienna, Austria).

Rossi, M., 1996. Morphology and mechanism of eruption of postglacial shield volcanoes in Iceland. Bull. Volcanol. 57 (7), 530–540.

Rossi, M., 1997. Morphology of the 1984 open-channel lava flow at Krafla volcano, northern Iceland. Geomorphology 20 (1–2), 95–112.

Rowland, S.K., Walker, G.P.L., 1987. Toothpaste lava: characteristics and origin of a lava structural type transitional between pahoehoe and aa. Bull. Volcanol. 52, 631–641.

Rowland, S.K., Walker, G.P.L., 1990. Pahoehoe and aa in Hawaii: volumetric flow rate controls the lava structure. Bull. Volcanol. 52, 615–628.

Self, S., Keszthelyi, L., Thordarson, T., 1998. The importance of pāhoehoe. Annual Review of Earth and Planetary Sciences 26 (1), 81–110.

Sigmarsson, O., Halldórsson, S.A., 2015. Delimiting Bárðarbunga and Askja volcanic systems with Sr- and Nd-isotope ratios. Jökull 65, 17–27.

Sigmundsson, F., et al., 2014. Segmented lateral dyke growth in a rifting event at Bárðarbunga volcanic system, Iceland. Nature. http://dx.doi.org/10.1038/nature14111.

Swanson, D.A., 1973. Pahoehoe flows from the 1969–1971 Mauna Ulu eruption, Kilauea volcano, Hawaii. Geol. Soc. Am. Bull. 84, 615–626.

Thordarson, T., Höskuldsson, A., 2008. Postglacial volcanism in Iceland. Jökull 58, 197–228.

Thordarson, T., Larsen, G., 2007. Volcanism in Iceland in historical time: volcano types, eruption styles and eruptive history. J. Geodyn. 43 (1), 118–152.

Thordarson, T., Self, S., 1998. The Roza Member, Columbia River Basalt Group: a gigantic pahoehoe lava flow field formed by endogenous processes? J. Geophys. Res. 103 (B11):27411–27445. http://dx.doi.org/10.1029/98JB01355.

Thordarson, T., Sigmarsson, O., 2009. Effusive activity in the 1963–1967 Surtsey eruption, Iceland: flow emplacement and growth of small lava shields. In: Thordarson, T., Self, S., Larsen, G., Rowland, S.K., Höskuldsson, A. (Eds.), Studies in Volcanology: The Legacy of George Walker. Special Publications of IAVCEI. 2. Geological Society, London, pp. 53–84.

Thordarson, T., Höskuldsson, A., Jónsdottir, I., Pedersen, G.B.M., Gudmundsson, M.T., Dürig, T., Riishuus, M.S., Moreland, W.M., Gudnason, J., Gallagher, C.R., Askew, R.A., 2015. Emplacement and Growth of the August 2014 to February 2015 Nornahraun Lava Flow Field North Iceland. AGU, San Francisco, USA.

Walker, G.P.L., 1991. Structure, and origin by injection under surface crust, of tumuli, "lava rises," "lava-rise pits," and "lava-inflation clefts" in Hawaii. Bull. Volcanol. 53, 546–558.